ASCA OBSERVATION OF THE DISTANT CLUSTER OF GALAXIES Cl 0016+16 AND IMPLICATION FOR H_0

A. FURUZAWA, Y. TAWARA, H. KUNIEDA, AND K. YAMASHITA

Department of Physics, Nagoya University, Furo-cho, Chikusa-ku, Nagoya 464-8602, Japan; furuzawa@u.phys.nagoya-u.ac.jp,
tawara@u.phys.nagoya-u.ac.jp, kunieda@u.phys.nagoya-u.ac.jp, yamasita@u.phys.nagoya-u.ac.jp

T. SONOBE AND Y. TANAKA

Institute of Space and Astronautical Science, 3-1-1 Yoshinodai, Sagamihara, Kanagawa 229-8510, Japan; sonobe@astro.isas.ac.jp, Y.Tanaka@sron.ruu.nl

AND

R. MUSHOTZKY

Laboratory for High Energy Astrophysics, NASA/GSFC, Greenbelt, MD 20771; richard@xray-5.gsfc.nasa.gov

ABSTRACT

We report the 0.5–10 keV X-ray image and spectrum of Cl 0016+16, which, at a redshift of 0.541, is one of the most distant clusters of galaxies observed with *ASCA*. The *ASCA* X-ray image is well represented by an isothermal β model. The best-fit parameters for the core radius (θ_c) and β are 0.'6 and 0.7, respectively. However, because of *ASCA*'s moderate spatial resolution, these two parameters are strongly correlated. The observed spectrum within a 6' radius is well fitted by a thin thermal emission model with a plasma temperature of 8.0 ± 1.0 keV. The Sunyaev-Zeldovich (SZ) effect in Cl 0016+16 has been observed by Carlstrom et al. using an interferometer and by Birkinshaw et al. using a single-dish radio telescope. Combining the SZ microwave decrement with the plasma density and temperature profiles derived from our X-ray observation, we obtained a value of the Hubble constant of 47 ± 14 km s^{-1} Mpc^{-1} with the profile parameters obtained by interferometric data, and 52 ± 20 km s^{-1} Mpc^{-1} with our best-fit shape parameters and single-dish telescope data.

Subject headings: cosmology: observations — galaxies: clusters: individual (Cl 0016+16) — X-rays: galaxies

1. INTRODUCTION

Cl 0016+16, at a redshift of 0.541 ± 0.001 (Koo 1981), is notable for its extreme richness and its absence of a dominant optical galaxy. The galaxy distribution of Cl 0016+16 shows a northeast-southwest elongation with an axial ratio of ~0.6 and a core radius of 46", and it is classified as Bautz-Morgan type II–III. Most galaxies within 3' are very red, and there is no indication of a relative excess of blue galaxies (the Butcher-Oemler effect; Koo 1981). *Einstein* and *ROSAT* (White, Silk, & Henry 1981; Hughes, Birkinshaw, & Huchra 1995; Neumann & Böhringer 1997) observations obtained a soft X-ray image and placed a lower bound on the plasma temperature of $kT > 6$ keV. We report the results of an observation obtained with the *ASCA* mission, the first satellite to have enough sensitivity to determine the plasma temperature of distant clusters.

Cl 0016+16 also shows the largest known Sunyaev-Zeldovich decrement of brightness temperature in the radio band (Carlstrom, Joy, & Grego 1996; J. E. Carlstrom 1997, private communication; Birkinshaw 1991; M. Birkinshaw 1997, private communication).

The Sunyaev-Zeldovich (SZ) effect arises from inverse Compton scattering of cosmic microwave background radiation by thermal electrons in the intracluster gas at temperature T_g (Sunyaev & Zeldovich 1981). This effect is observed as the reduction in the brightness of the microwave background radiation in the Rayleigh-Jeans region. The decrement of the brightness temperature (ΔT_r) is proportional to the product of the inverse Compton scattering depth through the cluster and the mean energy change of a scattering photon, which is proportional to the electron temperature, and the temperature difference can be written as

$$\frac{\Delta T_r}{T_r} \sim -\frac{2}{m_e c^2} \sigma_T 2 \int_0^\infty n_e(r) k T_g(r) dr , \tag{1}$$

where T_r is the temperature of the microwave background, n_e is the electron density, kT_g is the gas temperature, and σ_T is the Thomson cross section.

The thermal bremsstrahlung X-ray flux F_X from the cluster scales as

$$F_X \propto \frac{L_X}{D_L^2} \propto \frac{1}{D_L^2} \int_0^\infty n_e^2(r) k T_g^{1/2}(r) dV , \tag{2}$$

where V is the volume of the cluster, $n_e^2 kT_g^{1/2}$ is the bremsstrahlung emissivity, and D_L is the luminosity distance. Since the volume is proportional to $(D_A \theta)^2 l$, where l is the diameter of the cluster, D_A is the angular diameter distance, and θ is the angular size of the cluster, we will have D_A ($l = D_A \theta$) from equations (1) and (2). Assuming Ω_0 and q_0, H_0 can be derived from the relation between D_A and θ.

There are several ways to determine the absolute distance of objects and hence the Hubble constant. Among them, Cepheid variables are considered to be the most reliable classical distance indicator, but they are only observable in the nearest galaxies. Although the Tully-Fisher relation is applicable at considerably larger distances than Cepheid variables, even this method is limited to objects within a few hundred megaparsecs.

Deep *Hubble Space Telescope* (*HST*) observations have enabled the measurement of Cepheid distances of galaxies in the Virgo and Fornax clusters (Freedman et al. 1994). These results indicate a Hubble constant of $H_0 = 80 \pm 8$

Sensor	Exposure (s)	Count Rate (counts s^{-1})	Energy Band (keV)	Integration Radius (arcmin)
G2......	36,580	0.052	0.7–10	6
G3......	36,550	0.053	0.7–10	6
S0	26,400	0.061	0.5–10	5
S1	21,500	0.067	0.5–10	5

km s^{-1} Mpc^{-1}. However, the peculiar velocity of the observed galaxies is not negligible in comparison to the Hubble recession velocity, leading to a unknown additional uncertainty in H_0. Recently (Freedman 1997) these values have been slightly revised to 73 ± 4.

The use of the SZ effect (Sunyaev & Zeldovich 1981) is a fundamentally different way to derive the Hubble constant because it relies on the use of the basic physical process instead of the local calibration of empirical relationships.

A clear decrement of brightness temperature was found from several clusters (e.g., Cl 0016+16, A665, A2218, A2163, A773, and A1413; Birkinshaw, Gull, & Hardebeck 1984, Birkinshaw et al. 1991, Birkinshaw & Hughes 1994, Wilbanks et al. 1994, Grainge et al. 1993, 1996). X-ray observations of A665 and A2218 have been performed with *ROSAT* for the spatial distribution of the density and with *Ginga* for the temperature of hot plasma. They gave H_0 estimates of 51 ± 17 and 65 ± 25 km s^{-1} Mpc^{-1} (Birkinshaw et al. 1991; Birkinshaw & Hughes 1994). An *ASCA* observation of A2163 also gave an estimate of H_0 ranging between 42 and 100 km s^{-1} Mpc^{-1} (Markevitch et al. 1994, 1996).

In this paper we derive a value of H_0 based on X-ray spectral measurements of Cl 0016+16, one of the most distant cluster of galaxies detectable with *ASCA*.

2. OBSERVATION

The *ASCA* instrumentation consists of two gas imaging spectrometers (hereafter GIS2 and GIS3), two solid-state imaging spectrometers (hereafter SIS0 and SIS1), and four identical X-ray telescopes (XRTs) in front of each detector.

The XRT whose focal length is ~ 3.5 m consists of multinested conical thin foil X-ray mirrors (Serlemitsos et al. 1994). The effective areas of one XRT at 1 and 6 keV are ~ 290 and 153 cm^2, respectively. The XRT image quality can be characterized by a half-power diameter of 3'.

The GIS (Ohashi et al. 1996; Makishima et al. 1996), which is an imaging gas scintillation proportional counter, has good quantum efficiency in the energy band 1–16 keV ($>30\%$) and moderate energy resolution (7.8% FWHM at 6 keV), and covers a 30' radius field of view. The spatial resolution is about 0.5 at 6 keV.

The SIS, which consists of a 2×2 array of CCD chips, has very good energy resolution, 2% FWHM at 6 keV, and sensitivity in the energy band 0.5–9.5 keV (Burke et al. 1994). The position resolution is equal to the pixel size of 0.027 mm square. A CCD chip is ~ 11 mm square, and the field of view of SIS in 4 CCD mode is 22' square and in 2 CCD mode is $22' \times 11'$.

The observation of Cl 0016+16 was carried out on 1993 July 19 through 20 at the 2 CCD nominal position where the source image comes to the boundary of 2 of 4 chips of each SIS detector. The angular distance of Cl 0016+16

from the optical axis of each XRT is 3.4, 8.4, 6.0, and 6.2 for SIS0, SIS1, GIS2, and GIS3, respectively.

In order to avoid contamination of data by emission from the Earth's atmosphere and non–X-ray events, we selected the data acquired when the elevation angle was more than 25° from the bright Earth limb and more than 5° from the night Earth limb for SISs, more than 5° from the Earth limb for GISs, with a threshold cutoff rigidity of 6 GeV/c. The total resultant exposure time was $\sim 36,000$ s for GIS and $\sim 24,000$ s for SIS. Source count rates were ~ 0.05 counts s^{-1} for GIS and ~ 0.06 counts s^{-1} for SIS within a circle of 3' radius centered on the cluster. Details are listed in Table 1.

In the next section, we present the results of our analysis. In this paper all quoted errors are 90% confidence.

3. RESULTS

3.1. *X-Ray Images*

Figure 1a shows the X-ray image obtained with GIS2, and Figure 1b with SIS0. These images are not background subtracted. Note that the valley-like structure in Figure 1b running from northwest to southeast is due to lack of data at the boundary of 2 CCD chips. Figure 2 is the azimuthal averaged surface brightness distribution of the SIS0 image after background subtraction, based on the background map from the superposed blank fields accumulated in much longer exposures for the X-ray background observations. It is clear that Cl 0016+16 is more extended than the distribution expected for a point source (shown in Fig. 2; *solid line*).

An additional point source is seen 3.5 away from the cluster center, which coincides with the active galactic nucleus (AGN) HB89 0015+162. Thirty photons are found within the circle of 1' diameter centered at the AGN. Assuming that all these photons come from the AGN, its intensity is less than 0.003 counts s^{-1}. When we integrate the cluster flux within 6' radius, the contamination from this point source is estimated to be 5% based on a detailed ray tracing of the *ASCA* XRT spatial response function, and thus the AGN does not have a serious impact on the X-ray spectra or structure of the cluster.

For many X-ray–bright clusters of galaxies, the X-ray surface brightness distribution looks relatively axially symmetric and the radial profile is well fitted by the isothermal β model.

$$S(\theta) = S_0 \left(1 + \left(\frac{\theta}{\theta_c} \right)^2 \right)^{-3\beta + 0.5}, \qquad (3)$$

where θ_c is the X-ray core radius and S_0 is the central surface brightness.

Assuming isothermality and spherical symmetry, this brightness profile corresponds to the gas density distribution as follows

$$n_e(r) = n_0 \left(1 + \left(\frac{r}{r_c} \right)^2 \right)^{-3\beta/2}, \qquad (4)$$

where n_0 is the central gas density.

White et al. (1981) derived a core radius $\theta_c = 30''$ and central surface brightness $S_0 = 3.7 \times 10^{-4}$ ergs s^{-1} cm^{-2} from *Einstein* HRI data. However, because of the poor statistics, they fixed $\beta = 0.5$, which is inconsistent with the more recent data.

Recently, the *ROSAT* PSPC data for this cluster of galaxies was fitted by an isothermal β model with $\theta_c \sim 0.7$ and
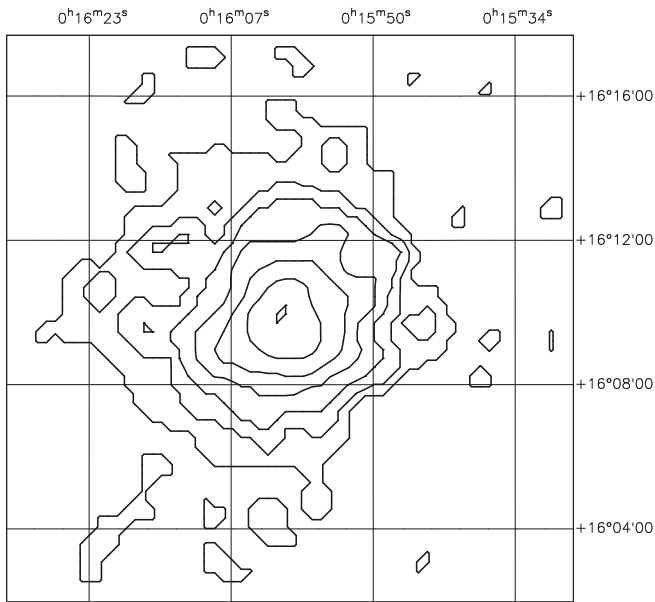
FIG. 1a
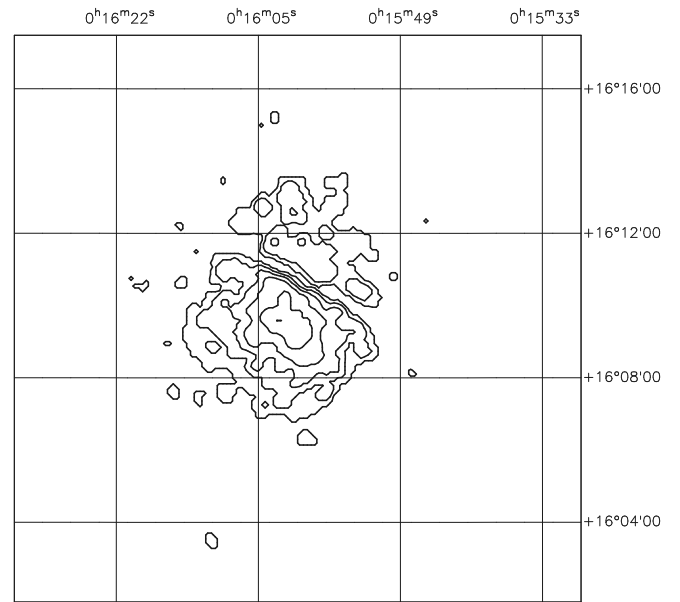
FIG. 1b

FIG. 1.—Image of the X-ray emission from Cl 0016+16 obtained (*a*) by GIS in the 0.7–10 keV band and (*b*) by SIS in the 0.5–10 keV band. These are convoluted with a Gaussian with $\sigma = 0\farcs5$ and $0\farcs2$, respectively. The lowest contour is drawn at twice the background level, and higher level contours are spaced by equal logarithmic intervals, which corresponds to a factor of 1.47.

$\beta \sim 0.74$ with better statistics (Hughes et al. 1995), or $\theta_c = 0\farcs83$ ($0\farcs72$–$0\farcs96$) and $\beta = 0.80$ (0.73–0.89) (Neumann & Böhringer 1997).

We fitted the *ASCA* radial profile obtained in the 0.5–10 keV energy range with the isothermal β model using the point-spread function (PSF) and vignetting derived from *ASCA* XRT ray-tracing simulations (Kunieda et al. 1995).

In Figure 3 the 90% and 99% confidence level contours are plotted against θ_c and β. The best-fit values obtained with *ASCA*, $\theta_c = 0\farcs6$ and $\beta = 0.64$ are consistent within the
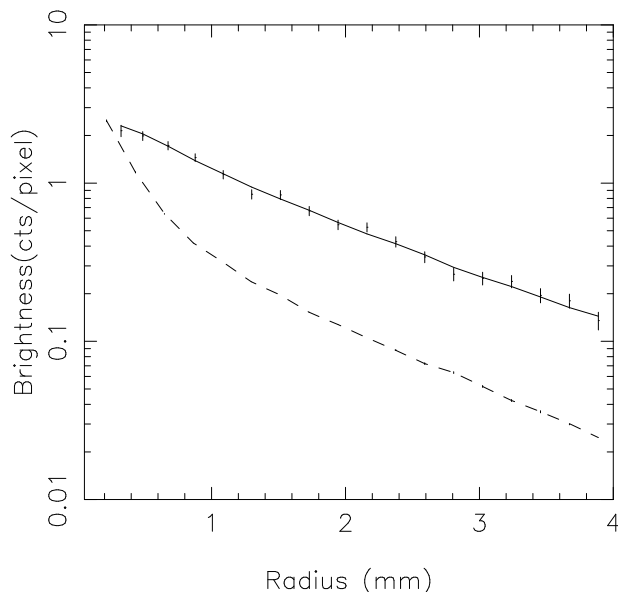
errors with those obtained from *ROSAT* PSPC. While the β model is a good fit to the overall X-ray image, the archival *ROSAT* PSPC image of Cl 0016+16 shows that it is slightly elliptical. A detailed analysis of the cluster by Neumann & Böhringer (1997) confirms this impression.

3.2. *X-Ray Spectra*

In order to get the cluster spectrum, the data within a 6′ radius, which includes $\sim 80\%$ of the flux of the whole cluster, is integrated. The spectrum obtained from each detector (energy band; 0.7–10 keV for GISs, 0.5–10 keV for SISs) are fitted with a collisional ionization equilibrium plasma emission model (Raymond & Smith code; Raymond & Smith 1977) with the neutral hydrogen absorption on the line of sight (Fig. 4) as a free parameter. The obtained parameters from each of the SIS and GIS detectors are consistent. The same spectral model is then applied to GIS2+GIS3 and SIS0+SIS1 independently. Although the best-fit N_H of $(1.4 \pm 1.0) \times 10^{21}$ cm^{-2} for GIS2+GIS3 is slightly larger than that for the SISs, the value of $(5.8 \pm 2.9) \times 10^{20}$ cm^{-2} obtained with SIS0+SIS1 is very close to the Galactic value of 5.0×10^{20} cm^{-2} derived from 21 cm data. Since the SIS has better sensitivity to N_H, the absorption column density is fixed at the Galactic value in the following fits. Then the temperature and abundance obtained from simultaneous fitting of GIS2+GIS3 and SIS0+SIS1 are $8.0^{+1.0}_{-0.8}$ keV and $0.11^{+0.12}_{-0.11}$ relative to the cosmic value [cosmic: $n(\mathrm{Fe})/n(\mathrm{H}) = 4.0 \times 10^{-5}$].

Our result is slightly dependent on the background subtraction method. There are two different methods to get background spectra. One is to use the background spectra integrated within a circle of 6′ radius in a source-free sky region of the present field of view. We picked three different positions at the same nominal off-axis angle for the 2 CCD mode observations. Another method is to use the spectrum from superposed blank field accumulated in a much longer

FIG. 2.—Radial profile of the observed surface brightness for Cl 0016+16 by SIS0. The solid line is the simulated profile with the best-fit parameters of the β model. The dashed line shows the expected radial profile for a point source.
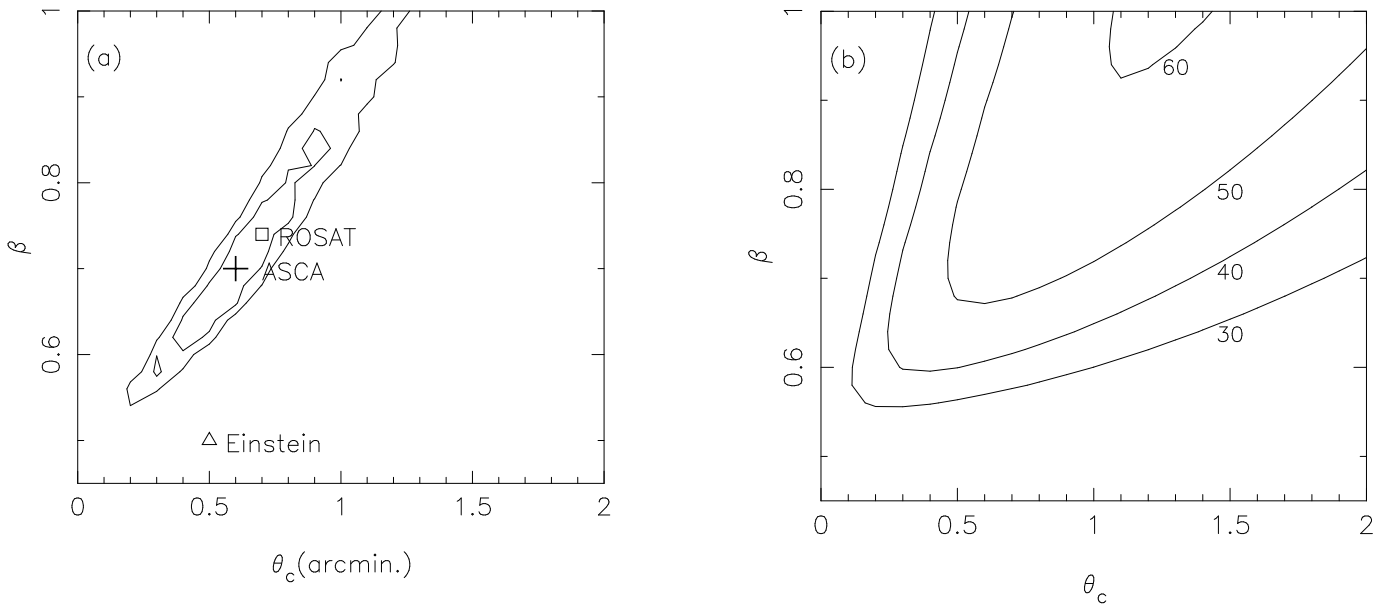
FIG. 3.—(a) Confidence level contours for (θ_c, β) obtained by the β model fitted to the SIS0 radial profile. Confidence level contours at 90% and 99% and the best-fit values obtained by *ASCA* (*plus sign*), *ROSAT* (Hughes's data; *square*), and *Einstein* (*triangle*) are plotted. (b) Contours of the value of the Hubble constant using Birkinshaw's data, corresponding to 50, 55, 60, 65, 70, 75, 80, 85, and 90 km s^{-1} Mpc^{-1}.

exposure from the cosmic X-ray background (CXB) observations. The temperatures from one of the detectors with four different background files showed 3.5% standard deviation. We used the background spectra from the CXB observations for the spectral analysis mentioned above, because it has the best statistics and the other methods show consistent results.

When we extend the radius of integration, there is a small decrease in the averaged temperature (Table 2). However, this variation is larger than the telescope response calibration error (~ 1 keV). Thus it cannot be concluded that

TABLE 2

FITTING RESULT
(INTEGRATION RADIUS DEPENDENCE)

Integration Region	kT (keV)
$R < 3'$	$10.0^{+2.3}_{-1.7}$
$R < 6'$	$8.0^{+1.0}_{-0.8}$
$R < 8'$	$7.4^{+1.2}_{-1.0}$
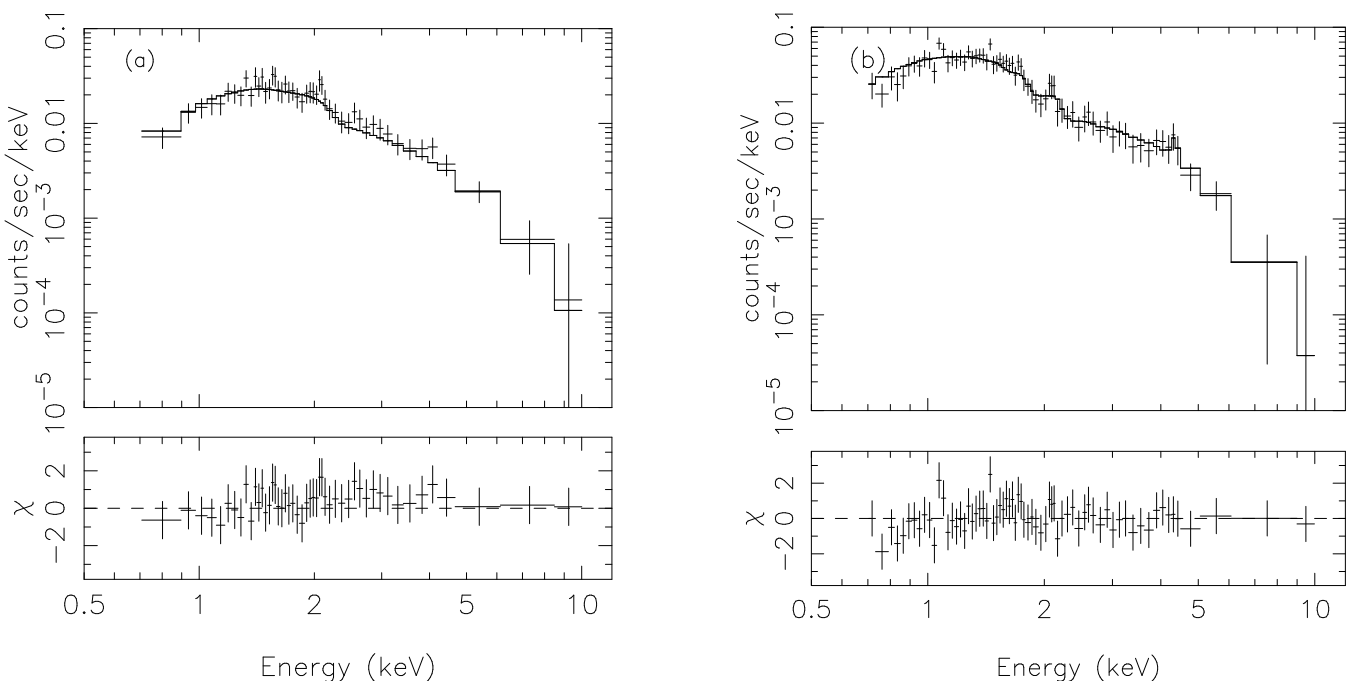
FIG. 4.—X-ray spectrum for Cl 0016 + 16 observed (a) by GIS and (b) by SIS. The solid line indicates the best-fitting spectrum, which corresponds to a thin hot plasma emission model in a collisional ionization equilibrium with $kT_g = 8.0$ keV.

there is a temperature gradient because of relatively large error bars in the present data set. Further investigation of the temperature distribution requires longer exposure observations. For the following spectral analysis, we use the data integrated within a 6' radius, because of the good statistics and the well-calibrated response of the telescope system.

As far as line features are concerned, the poor statistics still prevent us from obtaining definitive answers. For example, the iron line feature expected at 6.7 keV (rest frame) is not clearly seen. Since iron is the only element that is not fully ionized in such a hot plasma of several keV, its abundance is essentially decided by the equivalent width of the iron K line feature. However the upper limit of the Fe abundance quoted above is not inconsistent with that derived for other high-redshift clusters of galaxies (Mushotzky & Loewenstein 1997).

4. DISCUSSION

4.1. *Gas Temperature*

The best-fit temperature of $8.0^{+1.0}_{-0.8}$ keV in the present observation is well above the lower limit of 6 keV obtained from previous observations with *Einstein*. In general, the plasma temperature of clusters is highly correlated with X-ray luminosity; $L_X \propto kT^a$. If we use the 2–10 keV luminosity of 3.5×10^{45} ergs s^{-1} ($H_0 = 50$ km s^{-1} Mpc^{-1}, $q_0 = 0$), the plasma temperature of Cl 0016+16 is predicted to be about 10 keV, according to the correlation established for low-redshift ($z < 0.1$) clusters by *EXOSAT* medium-energy (ME) observations ($a = 3.57$; Edge & Stewart 1991) and by *Einstein* MPC, *EXOSAT* ME, *Ginga*, and *HEAO-1* observations ($a = 3.45$; David et al. 1993). Recently, a similar correlation between temperature and luminosity of clusters ($z < 0.4$) has been obtained with *ASCA* data (Tsuru et al. 1995; Kumada et al. 1996; Mushotzky & Scharf 1997). Its extrapolation also suggests a 10 keV temperature for Cl 0016+16. Preliminary *ASCA* results for distant clusters show no evolution in the L_X-kT relation (Mushotzky & Scharf 1997), but there is a ~2 keV scatter in the relationship which is consistent with the measured luminosity and temperature of Cl 0016+16.

4.2. *Spatial Distribution*

The core radius is strongly coupled with β for *ASCA* data because of the moderate spatial resolution of the *ASCA* XRT and the low signal-to-noise ratio (S/N) at large radii (~1 at $r > 6'$). The ROSAT best-fit value is quite consistent with the *ASCA* value, while the value from the *Einstein* HRI is not, probably because the HRI image is rather poor (see Fig. 1*a* of the paper by White et al. 1981). We will use the θ_c and β contours from *ASCA* or *ROSAT* for the density distribution to derive the Hubble constant. The *ASCA* X-ray flux result will be used, to be fully consistent with the values of the spectral parameters and because it does not depend on θ_c and β in contrast to the central surface brightness. The error of the X-ray flux due to the uncertainty of the intrinsic surface brightness distribution is definitely smaller than the flux calibration error (~10%) because of the small extent of Cl 0016+16.

From the detailed structure analysis of the surface brightness distribution using *ROSAT* PSPC data, this cluster seems to be slightly elongated (Hughes et al. 1995), and the ellipticities of isophotes of the X-ray image increase from zero near the center of Cl 0016+16 to a maximum of 0.24 at

a radius of 80'' before decreasing to zero again at 120''. From 120'' to 200'', the ellipticity lies in the range 0.05–0.1.

This ellipticity is similar to that seen in many low-redshift clusters (cf. Buote & Tsai 1996). If this cluster is a strong merger, one might expect the system to show a nonisothermal temperature structure (Markevitch 1996); however, our present data are not of sufficient quality or spatial resolution to show ellipticity and possible temperature structure. There is no evidence of a temperature gradient in the *ROSAT* PSPC data (Neumann & Böhringer 1997).

4.3. *Microwave Decrement Data*

Measurements of the microwave decrement in the direction of this cluster have been obtained by several authors (Birkinshaw et al. 1984; Uson 1987; Birkinshaw 1991; Birkinshaw 1997 [see footnote 1]; J. E. Carlstrom 1997, private communication). There are two different techniques to measure the decrement: an interferometric technique and a single-dish radiometric one. The newest result is based on an interferometric technique at 28.7 GHz (J. E. Carlstrom 1997, private communication). The newest result with a single-dish radiometer was obtained at 20 GHz by Birkinshaw (1997 [see footnote 1]).

The microwave decrement is proportional to the integrated gas pressure through the line of sight (eq. [1]). Then assuming the isothermal β model as a gas density and temperature distribution model, the model profile of the decrement can be expressed as

$$\Delta T_r(\theta) = \Delta T_{r0}\left(1 + \left(\frac{\theta}{\theta_c}\right)^2\right)^{(-3\beta+1)/2}, \qquad (5)$$

where ΔT_{r0} is a central decrement. Since an interferometric observation provides an image of the SZ effect, the central decrement ΔT_{r0} can be obtained by fitting the model to the image. J. E. Carlstrom (1997, private communication) obtained an image of the SZ effect with the millimeter array at Owens Valley Radio Observatory (OVRO) for Cl 0016+16. Their value of the central decrement is $\Delta T_{r0} = -1.20 \pm 0.12$ mK using the parameters of the β model, $\theta_c = 43\overset{''}{.}9$, $\beta = 0.74$, an ellipticity of 1.2, and a position angle of 60°, which were obtained by fitting the β model to the SZ image. Using the X-ray–derived parameters (Hughes et al. 1995), they also derived the central decrement of $\Delta T_{r0} = -1.23 \pm 0.12$ mK.[2]

Birkinshaw et al. (1984) observed the brightness temperature in the direction of this cluster at 20.3 GHz using the 40 m telescope at OVRO. In this observation, the directly measured value is integrated over the angular distribution of the decrement, which depends on the structure of the X-ray–emitting gas, with the primary beam pattern of the telescope (Gaussian beam with half-power width 107''). In order to derive a decrement at the center of this cluster, they assumed a decrement profile model derived from results of *Einstein* HRI observation (White et al. 1981). That model corresponds to the β model density profile with fixed β value of 0.5. This convolution gives a decrement of $\Delta T_{r0} = 1.40 \pm 0.17$ mK at the center of this cluster. However, Moffet & Birkinshaw (1989) found several radio sources in the field of view of the 40 m telescope at OVRO with the VLA. Correcting the OVRO data for the flux in the

---

[2] The value of the central decrement for Cl 0016+16 published in 1993 (Carlstrom et al. 1997) has been revised recently. The decrement reported for A773 in the same paper also should be corrected.

VLA sources, they revised the value of the central decrement to $\Delta T_{r0} = 1.20 \pm 0.19$ mK with using the model parameters $\theta_c = 0\overset{''}{.}68$ and $\beta = 0.73$ (including zero-level offset of the baseline microwave background near Cl 0016+16; M. Birkinshaw 1997, private communication).

In the case of radiometric data, the beam pattern of the telescope is simple and well known. Then we can recalculate ΔT_{r0} using equation (5) and the telescope beam pattern (see Birkinshaw & Gull 1984). The derived values of ΔT_{r0} are 1.26 ± 0.20 mK for the *ASCA* best-fit values of θ_c and β, and 1.23 ± 0.19 mK for the *ROSAT* best-fit values obtained by Hughes et al. (1995).

4.4. *Hubble Constant*

Combining the density profile and plasma temperature of X-ray–emitting gas, and the microwave decrement, the Hubble constant can be derived as shown in § 1. The intracluster gas distribution is assumed to be the isothermal β model. The microwave decrement is expressed precisely as

$$\frac{\Delta T_{r0}}{T_r} = \frac{2kT_g \sigma_T}{m_e c^2} r_c n_0 \sqrt{\pi} \frac{\Gamma(1.5\beta - 0.5)}{\Gamma(1.5\beta)} . \qquad (6)$$

The X-ray flux is

$$F_X = \frac{r_c^3 n_0^2 \Lambda(T_g)}{2D_L^2} \frac{\sqrt{\pi}}{2} \frac{\Gamma(3\beta - 1.5)}{\Gamma(3\beta)}, \qquad (7)$$

where $\Lambda(T_g)$ is the X-ray spectral emissivity in the observed 2–10 keV band. We used equation (6) in White & Silk (1980) as $\Lambda(T_g)$. Where $r_c = (c/H_0)[z(z/2 + 1)/(z + 1)^2]\theta_c(q_0 = 0)$, then the Hubble constant is

$$H_0 = \frac{cz(z/2 + 1)}{(z + 1)^2} \left(\frac{\Delta T_{r0}}{T_r}\right)^{-2}$$
$$\times \left[\frac{2kT_g}{m_e c^2} \sigma_T G(\beta)\right]^2 \frac{(1 + z)^4 F_{X2-10keV}}{\theta_c \Lambda(T_g)},$$
$$G(\beta) = \left[\frac{\sqrt{\pi}}{4} \frac{\Gamma(3\beta - 1.5)}{\Gamma(3\beta)}\right]^{-0.5} \sqrt{\pi} \frac{\Gamma(1.5\beta - 0.5)}{\Gamma(1.5\beta)} . \qquad (8)$$

Using the gas temperature and X-ray flux we obtained, we derive $H_0 = 47 \pm 14$ km s^{-1} Mpc^{-1} from Carlstrom's 1997 results ($\theta_c = 0\overset{''}{.}75$, $\beta = 0.74$, and $\Delta T_{r0} = -1.23 \pm 0.12$ mK) and $H_0 = 54 \pm 21$ km s^{-1} Mpc^{-1} from Birkinshaw's 1997 results ($\theta_c = 0\overset{''}{.}68$, $\beta = 0.73$, and $\Delta T_{r0} = -1.20 \pm 0.19$ mK).

Using the results of the radiometric observations, ΔT_{r0} with the *ASCA* and *ROSAT* best-fit values of θ_c and β, gives $H_0 = 52 \pm 20$ km s^{-1} Mpc^{-1} and 55 ± 21 km s^{-1} Mpc^{-1}, respectively. The errors in the X-ray flux, plasma temperature, and microwave decrement have been combined in quadrature. The error due to the uncertainty of the cluster shape is not included here. The errors arising from the plasma temperature, microwave decrement, and X-ray flux are 35%, 55%, and 10% of total value, respectively. The values obtained are summarized in Table 3.

After we finished our analysis, Hughes & Birkinshaw (1998) reported the determination of the Hubble constant using the X-ray property and the SZ effect for this cluster with the *ROSAT* PSPC image, the *ASCA* spectrum (only GIS), and data obtained by the OVRO 40 m telescope. They have analyzed the X-ray image and the one-dimensional profile of the radio decrement more completely. Our results for the plasma temperature, the density

TABLE 3
PARAMETERS FOR H_0 DERIVATION

z	T_r (K)	F_{X2-10} (10^{-12} ergs s^{-1} cm^{-2})	kT_g (keV)
0.541	2.74	1.64 ± 0.16 (*ASCA*)	8.0 ± 1.0 (*ASCA*)

θ_c, β	ΔT_r (mK)	H_0 (km s^{-1} Mpc^{-1})
0$\overset{''}{.}$75, 0.74 (interferometer)	-1.23 ± 0.12[a]	47 ± 14
0$\overset{''}{.}$68, 0.73 (assumed)	-1.20 ± 0.19[b]	54 ± 21
0$\overset{''}{.}$7, 0.74 (*ROSAT*)	-1.23 ± 0.19[c]	55 ± 21
0$\overset{''}{.}$6, 0.70 (*ASCA*)	-1.26 ± 0.20[c]	52 ± 20

[a] Interferometer.
[b] Radiometer; published value.
[c] Radiometer; recalculated.

profile, and the Hubble constant are very consistent with the results of their analyses.

Once θ_c and β have been well determined, H_0 can be calculated with an accuracy (the error in H_0 is less than 20 km s^{-1} Mpc^{-1}). However, the *ASCA* data are not capable of tightly constraining the gas distribution profile, as can be seen in the contour map of θ_c and β (Fig. 3). Using equation (8), we can draw the lines of constant H_0 in Figure 3 using only the radiometric data. (In the case of interferometric data, similar constraints can be derived if the raw data are available. However, it is impossible to calculate these from the published values.)

If one compares these contours, the *ASCA* data alone can restrict H_0 to lie between 35 and 60 km s^{-1} Mpc^{-1} at 90% confidence. Therefore, the possible range of H_0 is from $H_0 = 35 \pm 14$ km s^{-1} Mpc^{-1} to $H_0 = 60 \pm 23$ km s^{-1} Mpc^{-1} deduced from Birkinshaw's data. On the other hand, *ROSAT* gives a much smaller parameter range for θ_c and β. Using the *ROSAT* PSPC values from Neumann & Böhringer (1997) and their quoted uncertainties, the best-fit value of H_0 lies in the range from 50 to 57 km s^{-1} Mpc^{-1} with an additional uncertainty of ± 20 km s^{-1} Mpc^{-1} due to the uncertainty in kT, F_X, and ΔT_r.

Previously, H_0 has been determined using the SZ effect for several clusters: A2218, A665, and A773. Our result is consistent with these three results, and all are smaller than the value ~ 73 km s^{-1} Mpc^{-1} deduced by a variety of techniques based on optical data (viz., the planetary nebula luminosity function, galaxy light fluctuation data, the globular cluster luminosity function, and the early Hubble Cepheid results; Freedman 1997).

The SZ effect has been observed in several clusters at lower redshifts ($z < 0.1$): Coma, A2142, A478, A2256 (Myers et al. 1997). The results give a value of H_0 consistent with our results, although the value has a large error.

A possible discrepancy between the values of the Hubble constant derived from near and distant clusters can be produced by differences in the assumed cosmological model (Ω_0, Λ_0) (Kobayashi, Sasaki, & Suto 1996). Discrepancies between the SZ Hubble constant and that derived from other techniques could also be caused by the assumption of an isothermal and spherical ICM distribution.

A cluster which is elongated along the line of sight will have a larger decrement at the center of the cluster than a spherical cluster with similar gas density and temperature. Thus there may be a sampling bias in the SZ cluster sample

toward such objects, which would result in a bias toward lower values of H_0.

If the distant clusters that give $H_0 \sim 50$ are elongated along the line of sight with an axial ratio of ~ 1.3, the obtained H_0 is underestimated and the true H_0 is ~ 80.

Roettiger, Stone, & Mushotzky (1997) estimate the systematic uncertainty of H_0 due to a clumpy ICM in a simulated merging/postmerging cluster. They state that such clusters cause H_0 to be underestimated by as much as 35% with more typical values ranging from 10% to 25%.

Unfortunately, we do not know the magnitude of such an effect because a complete statistical study of X-ray brightness structure has not been done. A large statistical sample of SZ clusters is necessary to reduce the systematic uncertainty in H_0.

5. CONCLUSIONS

We have analyzed the *ASCA* spectra of Cl 0016+16 and determined a plasma temperature of 8 ± 1 keV. This is one of the most distant clusters for which the determination of plasma temperature has been made. Combining this result with the observed gas profile and microwave decrement and assumptions of isothermal and spherical gas distribution, we derived the best-fit values of the Hubble constant from *ASCA* data: $H_0 = 52 \pm 20$ km s^{-1} Mpc^{-1} with radiometric data and $H_0 = 47 \pm 14$ km s^{-1} Mpc^{-1} with interferometric data. Most of the statistical error arises from the uncertainty of the radio decrement. More accurate X-ray spectral observations which will require a considerably longer exposure observation will reduce these uncertainties, but the uncertainty due to the cluster structure remains. In order to reduce this uncertainty, detailed temperature maps are necessary. There is a strong indication from the very high velocity dispersion of this cluster combined with the *ASCA* temperature that this cluster is not relaxed (Hughes et al. 1995). If this is the case, the use of the isothermal approximation can lead to considerable errors (Roettiger et al. 1997).

REFERENCES

Birkinshaw, M. 1991, in Physical Cosmology, ed. Tran Thanh Van (Gif-sur-Yvette: Editions Frontières), 177
Birkinshaw, M., & Gull, S. F. 1984, MNRAS, 206, 359
Birkinshaw, M., Gull, S. F., & Hardebeck, H. 1984, Nature, 309, 34
Birkinshaw, M., & Hughes, J. P. 1994, ApJ, 420, 33
Birkinshaw, M., Hughes, J. P., & Arnaud, K. A. 1991, ApJ, 379, 466
Buote, D. A., & Tsai, J. C. 1996, ApJ, 458, 27
Burke, B. E., Mountain, R. W., Daniels, P. J., Cooper, M. J., & Dolat, V. S. 1994, IEEE Trans. Nucl. Sci., 41, 375
Carlstrom, J. E., Joy, M., & Grego, L. 1997, ApJ, 456, L75
David, L. P., Slyz, A., Jones, C., Forman, W., & Vrtilek, S. D. 1993, ApJ, 412, 479
Edge, A. C., & Stewart, G. C. 1991, MNRAS, 252, 414
Freedman, W. L. 1997, preprint (astro-ph/9706072)
Freedman, W. L., et al. 1994, Nature, 371, 757
Grainge, K., Jones, M., Pooley, G., Saunders, R., Baker, J., Haynes, T., & Edge, A. 1996, MNRAS, 278, L17
Grainge, K., Jones, M., Pooley, G., Saunders, R., & Edge, A. 1993, MNRAS, 265, L57
Hughes, J. P., & Birkinshaw, M. 1998, preprint (astro-ph/9801183)
Hughes, J. P., Birkinshaw, M., & Huchra, J. P. 1995, ApJ, 448, L93
Kobayashi, S., Sasaki, S., & Suto, Y. 1996, PASJ, 48, L107
Koo, D. C. 1981, ApJ, 251, L75
Kumada, A., Furuzawa, A., Tawara, Y., & Yamashita, K. 1996, in X-Ray Imaging and Spectroscopy of Cosmic Hot Plasmas, ed. F. Makino & K. Mitsuda (Tokyo: Universal Academy Press), 115
Kunieda, H., Furuzawa, A., Watanabe, M., & the XRT Team. 1995, *ASCA* News, 3, 3

Makishima, K., et al. 1996, PASJ, 48, 171
Markevitch, M. 1996, ApJ, 465, 1
Markevitch, M., Mushotzky, R. F., Inoue, H., Yamashita, K., Furuzawa, A., & Tawara, Y. 1996, ApJ, 456, 437
Markevitch, M., Yamashita, K., Furuzawa, A., & Tawara, Y. 1994, ApJ, 436, L71
Moffet, A. T., & Birkinshaw, M. 1989, AJ, 98, 1148
Mushotzky, R., & Loewenstein, M. 1997, ApJ, 481, L63
Mushotzky, R., & Scharf, C. A. 1997, ApJ, 482, L13
Myers, S. T., Baker, J. E., Readhead, A. C. S., Leitch, E. M., & Herbig, T. 1997, ApJ, 485, 1
Neumann, D. M., & Böhringer, H. 1997, MNRAS, 289, 123
Ohashi, T., et al. 1996, PASJ, 48, 157
Raymond, J. C., & Smith, B. W. 1977, ApJS, 35, 419
Roettiger, K., Stone, J. M., & Mushotzky, R. F. 1997, ApJ, 482, 588
Serlemitsos, P. J., et al. 1994, PASJ, 47, 105
Sunyaev, A. R., & Zeldovich, Ya. B. 1981, Astrophys. Space Sci. Rev., 1, 1
Tsuru, T., Koyama, K., Hughes, J. P., Arimoto, N., Kii, T., & Hattori, M. 1995, in UV and X-Ray Spectroscopy of Astrophysical and Laboratory Plasmas, ed. Y. Yamashita & T. Watanabe (Tokyo: Universal Academy Press), 375
Uson, J. 1987, in Proc. NRAO Greenbank Workshop 16, Radio Continuum Processes in Clusters of Galaxies, ed. C. O'Dea & J. Uson (Green Bank: NRAO), 255
White. S. D. M., & Silk, J. 1980, ApJ, 241, 864
White, S. D. M., Silk, J., & Henry, J. P. 1981, ApJ, 251, L65
Wilbanks, T. M., Ade, P. A. R., Fischer, M. L., Holzapfel, W. L., & Lange, A. E. 1994, ApJ, 427, L75